Available online at www.sciencedirect.com
SCIENCE DIRECT®
Engineering Fracture Mechanics 71 (2004) 2621–2633
Engineering Fracture Mechanics
www.elsevier.com/locate/engfracmech

Fracture toughness of thermoset composites reinforced by perfectly bonded impenetrable short fibers

Yu Qiao *, Xinguo Kong, Ernian Pan

Department of Civil Engineering, University of Akron, Akron, OH 44325-3905, USA

Received 20 June 2003; received in revised form 25 December 2003; accepted 6 February 2004

Abstract

The fracture toughness of brittle thermoset resins could be improved significantly by perfectly bonded tough, short fibers through both crack trapping and bridging effects. In this paper, the crack trapping effect was studied through the analysis of the change of strain energy associated with the crack propagation across a regular array of fibers, and the bridging effect was discussed based on the Andersson–Bergkvist model. The fracture resistance increases with the fiber volume fraction, and is independent of the elastic properties of the matrix, the crack length, and the cross-sectional diameter of the fibers.

Keywords: Crack trapping effect; Short-fiber reinforced composites; Brittle matrix; Fracture toughness; Cleavage cracking

1. Introduction

Many tough materials such as polycarbonate (PC) and polyester can be perfectly bonded with brittle thermoset resins that are of high adhesion. This technique has been widely applied to fabricate short-fiber reinforced composites (SFRC) with high fracture toughness. The toughening effect of the short fibers consists of the bridging effect and the crack trapping effect [1–5]. The bridging effect is considered extrinsic in the sense that it is related to the pullout process of the field of short fibers exposed in the fracture surface behind the crack front. The crack trapping effect, sometimes considered intrinsic since it occurs along the crack front, is related to the nonuniform nature of the crack front propagation.

Fig. 1 shows the cleavage front breaking through a regular array of perfectly bonded PC rods in an epoxy matrix [3]. With the increasing of the applied stress intensity, the crack front gradually penetrated between the PC rods and eventually bypassed them when the two parts of the crack front at both sides of a PC rod merged, somewhat similar with a dislocation line bypassing a precipitate particle. During the penetration process, at the crest of the sigmoidal cleavage front the local stress intensity was smaller than that at the concave part. Since at the verge of propagating the local stress intensity was equal to the

* Corresponding author. Tel.: +1-330-972-2426; fax: +1-330-972-6020.
E-mail address: yqiao@uakron.edu (Y. Qiao).

0013-7944/$ - see front matter © 2004 Elsevier Ltd. All rights reserved.
doi:10.1016/j.engfracmech.2004.02.007

Nomenclature

Δa	crack growth length
δ	critical crack opening displacement
μ	shear modulus of the matrix
$\underline{v}$	Poisson's ratio of the matrix
$\vec{\xi}$	coordinate system (ξ_1, ξ_2) in the crack plane
a_0	initial crack length
a_1	the crack length after crack growth
b	sample thickness
c	fiber volume fraction
D	cross-sectional diameter of the fibers
l	center-to-center distance of the short fibers
E	Young's modulus of the matrix
G_b	effective fracture work associated with the bridging effect
G_{compos}	fracture resistance of the short-fiber reinforced composite
G_f	critical energy release rate to overcome the fiber array
G_{matrix}	critical energy release rate of the matrix
G_R	crack growth "driving force" that equals the local fracture resistance
h	height of the arm of double cantilever beam specimen
K_1	stress intensity factor if the short fibers did not exist
K	local stress intensity along the arrested crack front
K_{ICf}	critical stress intensity factor to overcome the fiber array
R	cross-sectional radius of the fibers
P	crack opening load
$\vec{x}$	coordinate system (x_1, x_2) in the crack plane

toughness of the matrix, K_{ICm}, the average stress intensity at the crack tip should be higher. According to the experimental data, the PC rods could give a 2–4 fold rise of the fracture toughness over the neat epoxy resin.

This process was similar to the regular penetration problem discussed by Gao and Rice [6], which were further studied through the simulation of crack front profile by Bower and Ortiz [7,8]. When the crack tip stress intensity, κ, is relatively small, the experimental observation and the numerical results fit with each other quite well; but when κ is close to the critical value, the penetration depth predicted by the numerical simulation is somewhat larger (see Fig. 1). It was reported that if the size/spacing ratio of the short fibers is higher than 0.35, the Bower–Ortiz model is no longer valid [5], primarily due to the nonlinear effect of the interaction between the obstacles and the advancing crack front.

After the short fibers are bypassed, they are left behind the crack tip bridging the crack flanks together, resulting in the well-known R-curve. Eventually the short fibers will be pulled out and the crack propagation will reach a steady state. A number of models have been developed to relate the microstructure to the fracture toughness, among which the Andersson–Bergkvist model [9] is one of the simplest methods and can capture the bridging effect in brittle materials quite successfully.

In view of the above considerations and the fact that there is still no satisfactory model can be utilized to calculate the toughening effect of the short fibers in SFRC with high fiber volume fraction, in Section 2 below, we will develop a model for the cleavage front penetrating across a regular array of tough

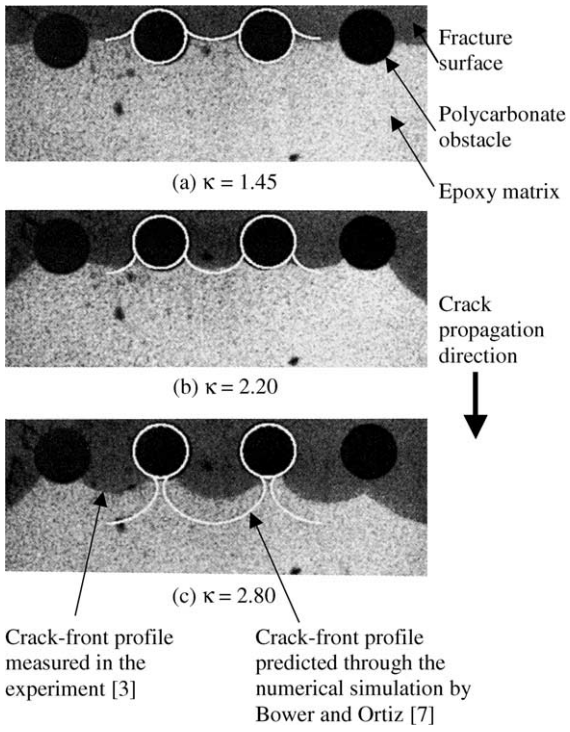

Fig. 1. Superposition of crack front profile predicted by the Bower–Ortiz model with digitized images of trapping in epoxy matrix by perfectly bonded polycarbonate obstacles [3], where κ is the applied stress intensity factor normalized by the critical stress intensity factor of the epoxy matrix.

fibers through an energy analysis. Then, in Section 3, the overall fracture toughness of SFRC will be discussed.

2. The resistance to cleavage cracking of a regular array of tough fibers

Consider the cleavage crack overcoming a regular array of perfectly bonded impenetrable fibers in the brittle thermoset matrix depicted in Fig. 2. The penetration depth of the front across the fiber array increases with the effective stress intensity at the crack tip. When the critical stress intensity K_{ICf}, or, equivalently, the critical energy release rate, G_{f}, for the front to surround the fibers is reached, the crack front bypasses the fibers and continues to advance, leaving the bridging fibers behind. To calculate the change of the strain energy associated with this break-through process, we assume that the crack is in a double cantilever beam (DCB) specimen with the initial crack tip at point "A_0", as depicted in Fig. 3a. It will be shown shortly that the geometry of the specimen has no influence on K_{ICf} and G_{f}.

The DCB specimen is homogeneous except for point "A" where the matrix is reinforced by a regular fiber array. As shown in Fig. 4, with increasing crack opening displacement δ, the crack opening load, P, first rises linearly from point "0" to point "1". When the critical stress intensity of the matrix, K_{ICm}, is reached, in ideal case where the crack growth is stable, P decreases smoothly along curve "1–2", until the crack tip is trapped by the fiber array at point "A". For the reason that will become clear, the critical stress intensity to break through the fiber array is higher than K_{ICm} and therefore P will increase linearly again to

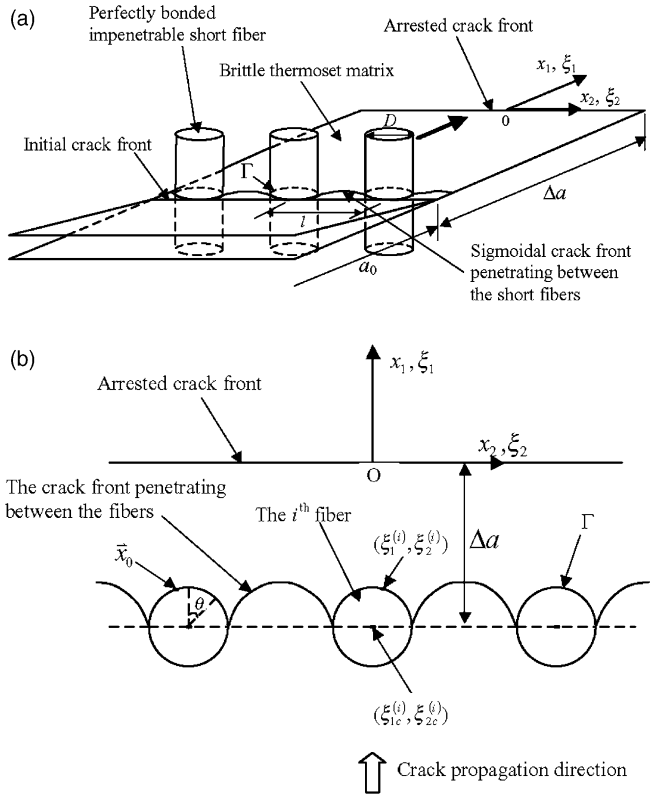

Fig. 2. Schematic diagrams of the cleavage crack front bypassing a regular array of perfectly bonded impenetrable short fibers in brittle matrix: (a) three-dimensional view; (b) top view.

point "3" where the cleavage front bypasses the fibers. Then, the crack propagates by a distance Δa to point "B" (see Fig. 3a–c), where the stress intensity at the crack tip decreases to K_{ICa}, the critical value to arrest the cleavage crack in the matrix, associated with the load drop from point "3" to point "4". During the crack growth, the variation of the crack opening displacement is negligible.

The change of the strain energy in the DCB specimen is due to the work of separation of the fracture surface and the dynamic energy dissipation. If Δa is much larger than the fiber radius R, the influence of short fibers on the profile of the arrested crack front is at negligible level, i.e. the crack front at point "B" can be assumed straight. Hence,

$$U_0 - U_1 = G_{\text{matrix}} \cdot \Delta a \cdot b + \widehat{U} \tag{1}$$

where U_0 and U_1 are the strain energies with the crack tip at "A" and "B", respectively; b is the specimen thickness; G_{matrix} is the critical energy release rate of the matrix; and $\widehat{U}$ is the dissipated kinetic energy associated with the dynamic effect [10]. The dynamic term, $\widehat{U}$, can be neglected if the crack growth is quasi-static, which can be achieved only when the local fracture resistance of the material equals the crack growth "driving force", G_R, along the crack path. Note that G_R is determined by the crack opening displacement and the bridging effect of the fibers, and therefore decreases as the crack front advances. Consequently, the local fracture resistance required to keep the crack growth quasi-static is position dependent. Under this condition,

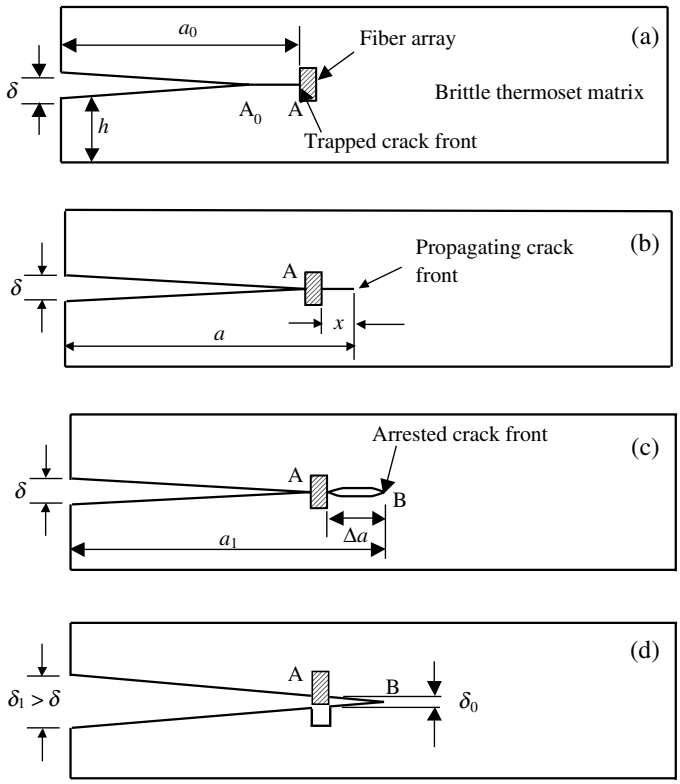

Fig. 3. Schematic diagram of the fracture process in a double cantilever beam sample of a thermoset reinforced by a fiber array: (a) before the crack overcomes the trapping effect of the fiber array; (b) the crack front bypasses the fiber array and advances in the matrix; (c) the front stops when the crack growth "driving force" decreases to G_{matrix}, leaving the bridging short fibers behind; and (d) eventually, with the increasing of the crack opening displacement, the short fibers are pulled out.

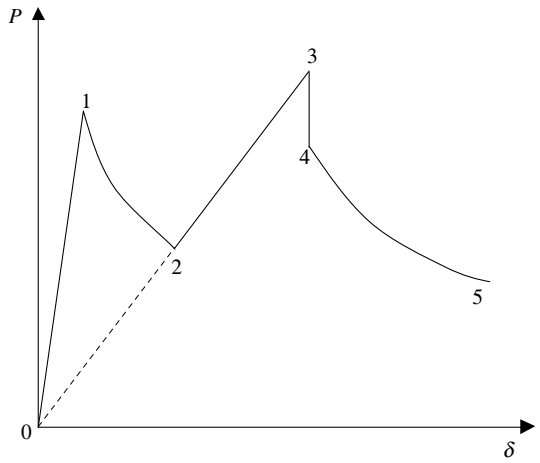

Fig. 4. Schematic diagram of the relationship between the crack opening load and the crack opening displacement in the fracture test of the double-cantilever beam specimen.

$$U_0 - U_1 = b\int_0^{\Delta a} G_R(x)\,dx \tag{2}$$

Note that there is no such a fracture resistance gradient from point "A" to point "B" in actual composites. However, since the ligament "A–B" is exposed to the fracture surface after the cleavage front has overcome the trapping effect of the fibers, and the properties of the material in front of the fiber array does not have influence on the front transmission, the value of G_f calculated in this "imaginary" case should be the same as the result of Eq. (1).

In the following discussion, U_0 and U_1 will be studied in context of basic beam theory. Because the influences of the shear stresses and free edges are only secondary, the improvement by using modified beam theories or finite element method is negligible. According to the basic beam theory,

$$U_0 = Ebh^3\delta^2/16a_0^3 \tag{3}$$

where E is the Young's modulus of the matrix, and h is the height of the DCB arm. The critical energy release rate of the fiber array is

$$G_f = -\frac{1}{b}\frac{\partial U}{\partial a} = \frac{3}{16}\frac{Eh^3\delta^2}{a_0^4} \tag{4}$$

with U being the strain energy and a being the crack length. Through Eq. (4), Eq. (3) can be rewritten as

$$U_0 = \frac{a_0 b}{3}G_f \tag{5}$$

If there were no short fibers at point "A", the energy release rate at the arrested crack tip would be

$$G^* = -\frac{1}{b}\frac{\partial U}{\partial a} = \frac{3}{16}\frac{Eh^3\delta^2}{a_1^4} \tag{6}$$

with $a_1 = a_0 + \Delta a$. Combination of Eqs. (4) and (6) gives

$$G_f = \left(\frac{a_1}{a_0}\right)^4 G^* = \left(\frac{a_1}{a_0}\right)^4 \frac{1-v^2}{E}K_1^2 \tag{7}$$

where $K_1 = \sqrt{EG^*/(1-v^2)}$.

Without the short fibers, the opening displacement at $\vec{x} = (x_1, x_2)$ is $\Lambda\widetilde{U}(\vec{x})$ [11,12] (see Fig. 2b), where

$$\widetilde{U}(\vec{x}) = 2K_1\cdot\sqrt{\frac{-x_1}{2\pi}} \tag{8}$$

and $\Lambda = \frac{1-v}{\mu}$, with v being the Poisson's ratio and μ being the shear modulus of the matrix. The displacement at $\vec{x}$ caused by a pair of unit bridging force at $\vec{\xi} = (\xi_1, \xi_2)$ is $\Lambda\widehat{U}(\vec{x}, \vec{\xi})$ [7,12], where

$$\widehat{U}(\vec{x}, \vec{\xi}) = \frac{1}{\rho\pi^2}\cdot \arctan\left\{2\sqrt{\frac{x_1\xi_1}{\rho^2}}\right\} \tag{9}$$

with $\rho = \sqrt{(x_1-\xi_1)^2 + (x_2-\xi_2)^2}$.

The crack opening displacement at the short fibers should be zero, i.e.

$$0 = \Lambda\widetilde{U}(\vec{x_0}) + \Lambda\int_\Gamma \widehat{U}(\vec{x_0}, \vec{\xi})\widetilde{P}(\vec{\xi})\,d\Gamma \tag{10}$$

where Γ is the matrix–fiber interface; $\vec{x_0} = (x_1^0, x_2^0)$ denotes any point in Γ; and $\widetilde{P}$ is the bridging stress distributed in Γ.

If the center-to-center distance of short fibers is comparable with the fiber diameter D, the bridging force at the matrix–fiber interface cannot be simplified as a concentrated force. Assume that the distribution of the bridging stress is the same in all the short fibers and the number of the short fibers is large, through $\tan\theta = \frac{\xi_2 - \xi_{2c}^i}{\xi_1 - \xi_{1c}^i}$, with (ξ_{1c}^i, ξ_{2c}^i) being the center of the ith fiber, Eq. (10) becomes

$$\int_0^{2\pi} P(\theta) g(\vec{x_0})\,\mathrm{d}\theta = c \tag{11}$$

where $P(\theta)$ is the bridging force at angle θ along the boundary of a short fiber; $c = K_1\sqrt{2\pi^3\Delta a}$; $g(\vec{x_0}) = \sum_{i=-\infty}^{+\infty} \frac{1}{\rho_i} \arctan\left(\frac{2\sqrt{x_1^0 \xi_1^{(i)}}}{\rho_i}\right)$; $\vec{\xi}^{(i)}$ is a point in the boundary of the ith short fiber; and ρ_i is the distance from $\vec{\xi}^{(i)}$ to $\vec{x_0}$. Note that in the above discussion, again, we assumed that Δa is much larger than D.

Eq. (11) is a Fredholm integral equation of the first kind, with the solution of

$$P(\theta) = \sum_n \lambda_n f_n y_n \tag{12}$$

where λ_n and y_n are the nth eigenvalue and eigenvector of $g(\vec{x_0})$, respectively, and $\sum_n f_n y_n = c$.

With the bridging force P, the stress intensity along the arrested crack front is [7]

$$K(x_2) = K_1 + \int_\Gamma H(s, \vec{\xi}) P(\theta)\,\mathrm{d}\Gamma \tag{13}$$

where $H(s, \vec{\xi}) = \sqrt{\frac{2}{\pi^3}} \frac{\sqrt{-\xi_1}}{s^2 + \xi_1^2}$ is the stress intensity at s due to a pair of unit bridging forces at $\vec{\xi}$, with s being $|x_2 - \xi_2|$. The average stress intensity factor and the average energy release rate of the arrested crack front can then be obtained as

$$\overline{K} = \frac{1}{l} \int_0^l K(x_2)\,\mathrm{d}x_2 \tag{14}$$

$$\overline{G} = (1 - \nu^2)\overline{K}^2/E \tag{15}$$

with l being the center–center distance of the short fibers. In the quasi-static case, $K_{\mathrm{ICa}} = K_{\mathrm{ICm}}$, and thus when the crack tip is arrested at point "B"

$$G_{\mathrm{matrix}} = \overline{G} = (1 - \nu^2)\overline{K}^2/E \tag{16}$$

Substitution of Eq. (14) into (16) gives

$$G_{\mathrm{matrix}} = \frac{1 - \nu^2}{El^2}\left[K_1 l + \int_\Gamma P(\theta)\widehat{H}(\vec{\xi})\,\mathrm{d}\Gamma\right]^2 \tag{17}$$

where $\widehat{H}(\vec{\xi}) = \int_0^l H(s, \vec{\xi})\,\mathrm{d}x_2$.

The quasi-static crack growth "driving force", $G_{\mathrm{R}}(x)$, can be obtained through the similar procedure with the calculation of $\overline{G}$. In the context of basic beam theory, if the bridging fibers did not exist, the stress intensity at the propagating crack tip at x is

$$K_{x1} = K_1\left(\frac{a_1}{a_0 + x}\right)^2 \tag{18}$$

Similar with the discussion of Eq. (11), the distributed bridging force, $P_x(\theta)$, required to close the fracture surface locally along the fiber–matrix interface is determined by

$$\int_0^{2\pi} P_x(\theta)\cdot g(\vec{x}_0)\,\mathrm{d}\theta = K_{x1}\sqrt{2\pi^3 x} \tag{19}$$

and the stress intensity along the crack front can then be stated as

$$K_x = K_{x1} + \int_\Gamma H(s,\vec{\xi})\cdot P_x(\theta)\,\mathrm{d}\Gamma \tag{20}$$

Thus, the average energy release rate at the crack tip is

$$G_{\mathrm{R}}(x) = (1-v^2)\overline{K}_x/E \tag{21}$$

where $\overline{K}_x = \frac{1}{l}\int_0^l K_x(x_2)\,\mathrm{d}x_2$.

When the crack tip is arrested at point "B", the additional strain energy associated with the bridging effect can be obtained as:

$$U_{\mathrm{bridging}} = \frac{b}{l}\left\{\frac{1}{2}\int_\Gamma P(\theta)\left[\Lambda\widetilde{U}(\vec{x})\right]\mathrm{d}\Gamma\right\} = \frac{bK_1}{l}\frac{1-v}{\mu}\int_\Gamma P(\theta)\sqrt{\frac{-x_1}{2\pi}}\mathrm{d}\Gamma$$

Note that the strain energy subsequent to the crack growth is

$$U_1 = U_1^* + U_{\mathrm{bridging}} \tag{22}$$

with $U_1^* = a_1 bG^*/3$ being the strain energy if the fiber array did not exist. Combination of Eqs. (2), (12), (17) and (22) gives $G_{\mathrm{f}}/G_{\mathrm{matrix}}$ and $\Delta a/D$ as functions of D/l.

Because it is impossible to obtain the analytical solution of y_n in Eq. (12), iteration method was applied to calculate G_{f} numerically through the Ritz method by assuming that $P(\theta)$ is of the form

$$P(\theta) = \begin{cases} P_0 + P_1\cdot\theta + P_2\cdot\theta^2, & 0\leqslant\theta\leqslant\pi, \\ P_0 - P_1\cdot\theta + P_2\cdot\theta^2, & -\pi\leqslant\theta\leqslant 0, \end{cases} \quad -\infty\leqslant i\leqslant +\infty \tag{23}$$

where P_0, P_1 and P_2 are unknown variables. The singularity integration involved in Eq. (12) was solved through the coordinate transformation method discussed by Pan and Amadei [13]. In the calculation of Eq. (19), $P_x(\theta)$ was assumed uniform to simplify the numerical procedure.

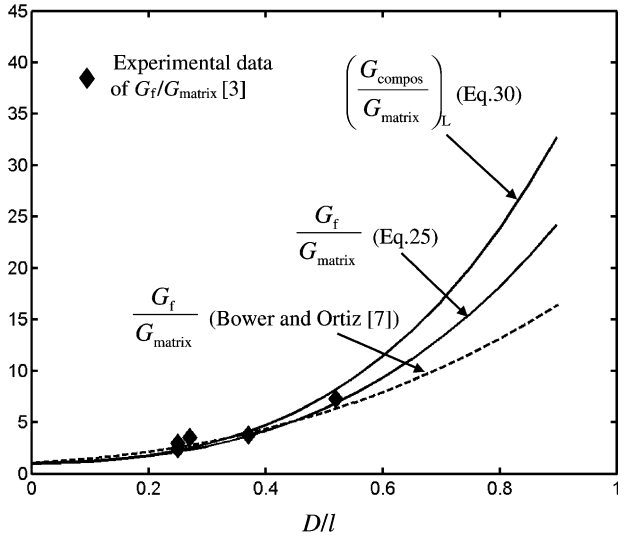

Fig. 5. Fracture resistance as function of size/spacing ratio.

Fig. 5 shows the results of G_f as function of D/l, which fit with the experimental data [3] quite well. Rose [14] has derived the exact solution of the toughening effect, G_{trap}, of a regular array of penetrable obstacles

$$\frac{G_{trap}}{G_{matrix}} = \left(1 - \frac{D}{l}\right) + \left(\frac{G_{obs}}{G_{matrix}}\right)\frac{D}{l} \tag{24}$$

where G_{obs} is the critical energy release rate of the reinforcing fibers. In this framework, the numerical results of Eqs. (2), (12), (17) and (22) can be regressed as

$$\frac{G_f}{G_{matrix}} = \left(1 - \frac{2R}{l}\right) + \left(1.0 + 9.6\frac{R}{l} + 1.8\frac{R^2}{l^2}\right)^2 \cdot \frac{2R}{l} \tag{25}$$

The term $(1.0 + 9.6\frac{R}{l} + 1.8\frac{R^2}{l^2})^2$ reflects $\frac{G_{fiber}^{(cr)}}{G_{matrix}}$, with $G_{fiber}^{(cr)}$ being the critical toughness for the fiber to become impenetrable.

3. The fracture toughness of short-fiber reinforced composites

After the crack bypasses the fiber array, the perfectly bonded short fibers are left behind the crack front, bridging the fracture flanks together. With the increasing of the applied stress intensity they will eventually be pulled out (see Fig. 3d). At the steady state, the additional fracture work associated with this bridging effect can be estimated through the Andersson–Bergkvist model [9]

$$G_b = \frac{\sigma_0\delta_0}{2} \cdot \frac{\pi D^2/4}{l^2} = \frac{\pi}{8}\frac{D^2}{l^2}(\sigma_0\delta_0) \tag{26}$$

where σ_0 is the maximum bridging stress, and δ_0 is the maximum bridging distance. Note that Eq. (26) gives only the first-order estimation of G_b. More accurate result can be obtained through the advanced process-zone models e.g. [15,16].

The overall fracture toughness of SFRC can be stated as

$$G_{compos} = G_f + G_b \tag{27}$$

Substitution of Eqs. (25) and (26) into (27) gives

$$\frac{G_{compos}}{G_{matrix}} = \left(1 - \frac{2R}{l}\right) + \left(1.0 + 9.6\frac{R}{l} + 1.8\frac{R^2}{l^2}\right)^2 \cdot \frac{2R}{l} + \chi_0\frac{R^2}{l^2} \tag{28}$$

where $\chi_0 = 4\pi\sigma_0\delta_0/8G_{matrix}$. If the value of $\sigma_0\delta_0$ is estimated based on $G_{fiber}^{(cr)}$ [13],

$$\chi_0 = \frac{\pi}{8}\left(\frac{P_{ave}}{G_{matrix}}\right) = \frac{\pi}{8}\left(1.0 + 9.6\frac{R}{l} + 1.8\frac{R^2}{l^2}\right)^2 \tag{29}$$

Thus, Eq. (28) becomes

$$\left(\frac{G_{compos}}{G_{matrix}}\right)_L = \left(1 - \frac{D}{l}\right) + \left(1.0 + 4.8\frac{D}{l} + 0.5\frac{D^2}{l^2}\right)^2 \cdot \left(\frac{D}{l} + \frac{\pi}{32}\frac{D^2}{l^2}\right) \tag{30}$$

Eq. (30) gives the lower limit of the critical energy release rate of thermoset composites reinforced by perfectly bonded impenetrable short fibers, which is shown in Fig. 5. It can be seen that when D/l is above 0.3, the bridging effect is much less pronounced compared with the crack trapping effect.

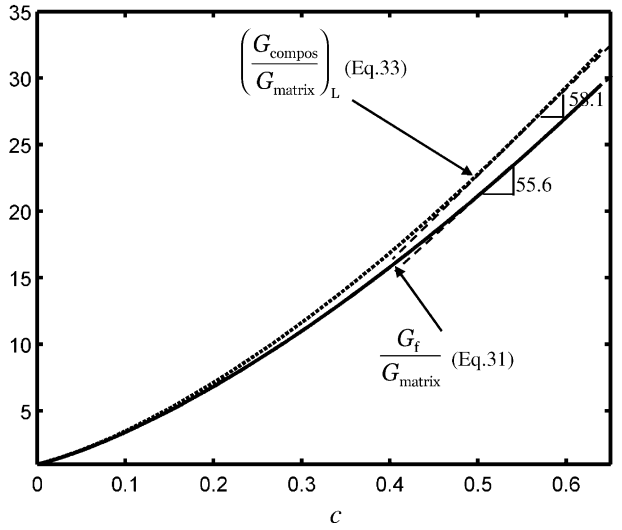

Fig. 6. Fracture resistance as function of fiber volume fraction.

The volume fraction of circular short fibers is $c = \frac{\pi D^2}{4l^2}$. Hence, Eqs. (25) and (26) can be rewritten as

$$\frac{G_f}{G_{matrix}} = (1 - 1.1\sqrt{c}) + \left(1.0 + 5.4\sqrt{c} + 0.6c\right)^2 \cdot (1.1\sqrt{c}) \tag{31}$$

$$\frac{G_{compos}}{G_{matrix}} = (1 - 1.1\sqrt{c}) + \left(1.0 + 5.4\sqrt{c} + 0.6c\right)^2 \cdot \sqrt{c} + \chi_1 c \tag{32}$$

where $\chi_1 = 1.3\chi_0$. Through the analysis similar to the discussion of Eq. (30), the lower limit of the overall fracture toughness can be estimated as

$$\left(\frac{G_{compos}}{G_{matrix}}\right)_L = \left(1 - 1.1\sqrt{c}\right) + \left(1.0 + 5.4\sqrt{c} + 0.6c\right)^2 \cdot (1.1\sqrt{c} + 0.1c) \tag{33}$$

Fig. 6 shows G_f/G_{matrix} and $(G_{compos}/G_{matrix})_L$ as functions of c. It can be seen that in the range of c from 0.45 to 0.65 $d(G_f/G_{matrix})/dc$ is nearly constant 55.6, and $d(G_{compos}/G_{matrix})_L/dc$ is nearly constant 58.1. With the constant fiber volume fraction, changing fiber diameter has little influence on the overall fracture toughness.

4. Discussion

Since in Eqs. (12), (17), (22) the parameters of the DCB specimen, b and h, vanish, the numerical results are independent of the specimen geometry. Although in these equations the initial crack length comes in by affecting both the rate of descending of the energy release rate and the ligament length Δa, through Table 1

Table 1
The numerical result of G_f/G_{matrix} as function of the initial crack length (a_0) and the fiber size/spacing ratio (R/l)

a_0/R	$R/l = 0.1$	$R/l = 0.2$	$R/l = 0.3$
10	1.6	4.5	9.9
100	1.6	4.4	9.8
1000	1.6	4.5	9.8

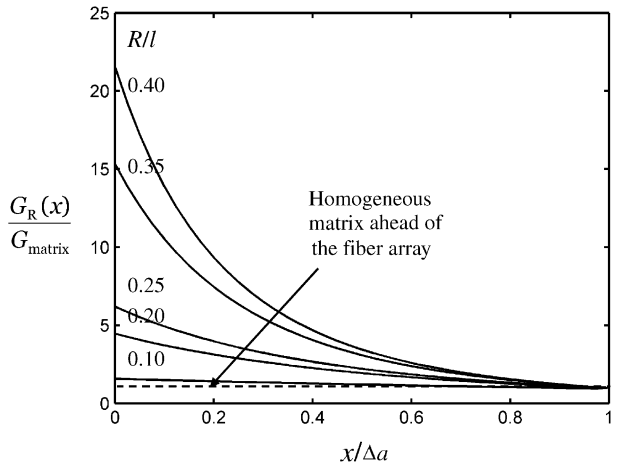

Fig. 7. The required fracture resistance gradient ahead of the fiber array to keep the crack growth quasi-static.

it can be seen that G_f is insensitive to a_0, i.e. the fracture resistance of SFRC is a material constant, as it should. Note that if the crack length is smaller than $10D$, the number of fibers encountered by the crack front is small and thus this model is no longer valid.

Fig. 7 shows the required fracture resistance gradient ahead of the fiber array to keep the crack growth quasi-static. In actual materials, in the ligament "A–B" (see Fig. 3), the fracture resistance is constant G_{matrix}. The difference between the two cases indicates the degree of importance of the dynamic effect. Comparison of Eqs. (1) and (2) shows that

$$\widehat{U} = b\int_0^{\Delta a}(G_R(x) - G_{matrix})\,dx \tag{34}$$

The energy radiated from the crack tip and eventually dissipated in the background, $\widehat{U}$, increases with the fiber size/spacing ratio, and this dynamic effect is more pronounced immediately subsequent to the crack front transmission across the fiber array than as the crack tip approaches point "B".

For isotropic materials, $E/E\mu = 2(1+v)$. Therefore, among the elastic parameters of the matrix including the modulus of elasticity E, the shear modulus μ, and the Poisson's ratio v, Eqs. (12), (17) and (22) are only related to v. Fig. 8 shows the effect of Poisson's ratio on G_f/G_{matrix}. In the range of 0.03–0.47, its influence is at negligible level. Since the Poisson's ratio of most of the engineering materials falls in this range, it can be stated that G_f is independent of the elastic properties of matrix.

As discussed above, through the simulation of the crack front profile, Bower and Ortiz obtained that [5,7,8]

$$\frac{G_f}{G_{matrix}} = \left(1 - \frac{D}{l}\right) + \left(2.1 + 2.4\frac{D}{l}\right)^2 \cdot \frac{D}{l} \tag{35}$$

The results of Eqs. (25) and (34) are compared in Fig. 5. They are about the same when D/l is below 0.5; if D/l is larger, the result of Eq. (25) is significantly higher, as it should. Since in Eq. (25) the complicated simulation of the penetration process of crack front is avoided and the distributed bridging force is calculated in detail, the result is valid when the D/l ratio is high.

Because it was assumed that debonding occurs only after the crack trapping effect is fully overcome, the effective work of separation of the fiber–matrix interface has no influence on G_f. However, it does affect the bridging effect G_b, which was captured by χ_0 in Eq. (28). The stronger the fiber–matrix interface, the larger the G_b, so does the overall fracture resistance G_{compos}. The minimum interface strength at which the

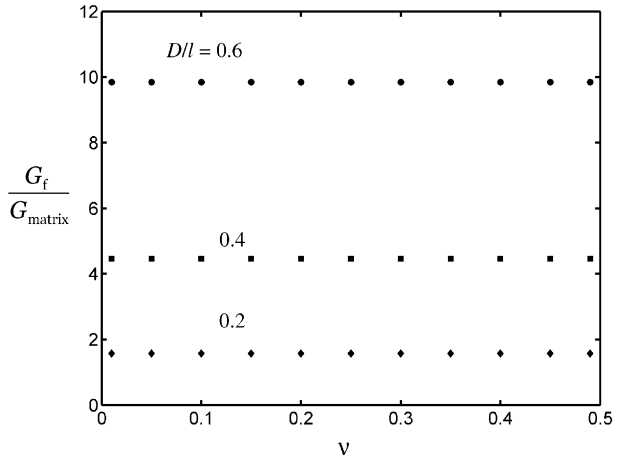

Fig. 8. The influence of Poisson's ratio on crack trapping effect.

interface can be considered as perfectly bonded during the penetration process is given by Eq. (30). Note that in the above discussion the fracture toughness was calculated based on the strain energy change instead of the stress/strain distribution at the crack tip and as a result the fracture mode mixity was ignored.

5. Conclusions

In this paper the toughening effect of perfectly bonded impenetrable short fibers in brittle thermoset matrix is studied. The fibers are assumed straight and well aligned in regular arrays. The improvement of the overall fracture toughness is attributed to the crack trapping effect and the bridging effect. Based on the comparison of the strain energy prior to and subsequent to the front transmission across a regular array of short fibers, the critical energy release rate G_f is calculated. By incorporating the effective fiber toughness into the framework of Rose model, the numerical results are regressed as Eq. (25). The bridging effect is studied based on the Andersson–Bergkvist theory, and the following conclusions are drawn:

(1) When the fiber volume fraction is low, the effects of crack trapping and bridging are comparable to each other; when the center-to-center distance of short fibers is relatively small, the crack trapping effect is much more important.
(2) When the matrix–fiber bonding is high enough such that debonding does not occur until the crack trapping effect is fully overcome, the overall fracture toughness increases with the fiber volume fraction. If the fiber volume fraction, c, is larger than 0.45, the relationship between the fracture resistance and c is nearly linear.
(3) If the fiber volume fraction is constant, changing fiber diameter have little influence on the overall fracture toughness.
(4) The resistance of SFRC to cleavage cracking is independent of the crack length and the elastic properties of matrix.

Acknowledgements

Special thanks are due to the reviewers of this paper for the valuable suggestions of the validity of assumptions.

References

[1] Low IM, Mai YW, Bandyopadhayay S. Effects of temperature and rate on fracture toughness of short alumina fiber reinforced epoxies. Compos Sci Tech 1992;43:3–12.
[2] Zhou LM, Kim JK, Baillte C, Mai YW. Fracture mechanics analysis of the fiber fragmentation test. J Compos Mater 1995;29:881–902.
[3] Mower TM, Argon AS. Experimental investigations of crack trapping in brittle heterogeneous solids. Mech Mater 1995;19:343–64.
[4] Belnap JD, Shetty DK. Micromechanics of crack bridging in sapphire epoxy composites. Compos Sci Tech 1998;58:1763–73.
[5] Xu G, Bower AF, Ortiz M. The influence of crack trapping on the toughness of fiber reinforced composites. J Mech Phys Solids 1998;46:1815–33.
[6] Gao H, Rice JR. A first-order perturbation analysis of crack trapping by arrays of obstacles. J Appl Mech 1990;56:828–36.
[7] Bower AF, Ortiz M. A three dimensional analysis of crack trapping and bridging by tough particles. J Mech Phys Solids 1991;39:815–58.
[8] Bower AF, Ortiz M. The influence of grain size on the toughness of monolithic ceramics. Trans ASME 1993;115:228–36.
[9] Andersson H, Bergkvist H. Analysis of a nonlinear crack model. J Mech Phys Solids 1970;18:1–28.
[10] Freund LB. Dynamic Fracture Mechanics. Cambridge University Press; 1998.
[11] Qiao Y. Unstable crack advance across a regular array of short fibers in brittle matrix. Compos Sci Tech 2004;64:711–7.
[12] Ulfyand YS. Survey of articles on the application of integral transforms in theory of elasticity. Raleigh, NC: University of North Carolina; 1965.
[13] Pan E, Amadei B. Fracture mechanics analysis of cracked 2-D anisotropic media with a new formulation of the boundary element method. Int J Fract 1996;77:161–74.
[14] Rose LRF. Toughening due to crack-front interaction with a second-phase dispersion. Mech Mater 1987;6:11–5.
[15] Meda G, Steif PS. A detailed analysis of cracks bridged by fibers. 1. Limiting cases of short and long cracks. J Mech Phys Solids 1994;42:1293–321.
[16] Rubinstein AA, Wang P. The fracture toughness of a particulate-reinforced brittle matrix. J Mech Phys Solids 1998;46:1139–54.